Dipteran-insect-inspired thoracic mechanism with nonlinear stiffness to save inertial power of flapping-wing flight

Lau, Gih-Keong; Chin, Yao-Wei; Goh, Joel Tian-Wei; Wood, Robert J.

2014

Lau, G.-K., Chin, Y.-W., Goh, J. T.-W., & Wood, R. J. (2012). Dipteran-insect-inspired thoracic mechanism with nonlinear stiffness to save inertial power of flapping-wing flight. IEEE transactions on robotics, 30(5), 1187-1197.

https://hdl.handle.net/10356/106240

https://doi.org/10.1109/TRO.2014.2333112

This is a pre-print version. The paper published appears in the IEEE TRANSACTIONS ON ROBOTICS, VOL. 30, NO. 5, OCTOBER 2014, pp. 1187 - 1197

Dipteran-Insect Inspired Thoracic Mechanism with Non-Linear Stiffness to Save Inertial Power of Flapping-Wing Flight

Gih-Keong Lau [1], Yao-Wei Chin [1], Joel Tian-Wei Goh [1], Robert J. Wood [2]
[1]School of Mechanical and Aerospace Engineering, Nanyang Technological University, Singapore 639798
[2]Harvard Microrobotics Laboratory, Harvard University, Cambridge, MA 02138 USA,

***Abstract*— This paper presents the design, analysis and characterization of a compliant thoracic mechanism that saves inertial power for flapping-wing micro-air vehicles (FWMAV). Lightweight polyimide film hinges were previously integrated in compliant flapping-wing mechanism to reduce friction. However, there were not stiff enough to fully recover wing's inertial energy into elastic energy. To store adequate elastic energy using film hinges, we develop a compliant thoracic mechanism with nonlinear stiffness characteristics by mimicking a Dipteran insect's flight thorax. This thoracic mechanism consists of rigid plates and polyimide film hinges, connected into a close-form shell. It has a nonlinearly increasing stiffness so that it can slow the wings down rapidly towards the end stroke and subsequently helps reverse the wings. It demonstrates almost full recovery of inertial power for 10-cm span flapping wings up to 25Hz. As a result, it only expends 2% of the total mechanical power on inertial power at 25Hz. In contrast, the rigid-body mechanism with no elastic storage expends 23% of the total mechanical power on inertial power when the same wings beat at the same frequency. With the capability of elastic energy storage, this compliant thoracic mechanism saves power expenditure ranging from 20% up to 30% to produce the same thrust, in comparison with the rigid-body flapping mechanism. This study shows that power saving is effective only if elastic energy storage is well tuned to recover the wing inertial power.**

I. INTRODUCTION

Natural flyers capable of agile maneuvers have inspired recent development of flapping-wing micro air vehicles. However, flapping-wing flight could be energetically costly during hovering [1][2]. Substantial power is expended to move the air and wings [3][4]. While aerodynamic power is incurred to produce aerodynamic thrust and lift, additional inertial power is needed to accelerate and decelerate wings[1][4]. Even for natural flyers, this inertial power increases greatly with increasing frequency and can take up as much as 53% of the total flight power during hovering [5]. However, entomologists and aerodynamicists found that insects have a way to reduce the inertial power by utilizing elastic energy storage during flapping-wing flight[2][6][7]. Insects have elastic elements in their flight muscles [8], flight thorax, and wing hinges[2][3]. At the end of wing stroke, kinetic energy from the flapping wings is stored as elastic energy in the deformed elastic elements and it is recovered subsequently during wing stroke reversal[3][9]. Hence, the insects' flapping-wing flight can be energetically efficient by eliminating energy expenditure on reactive power.

Contrary to natural flyers, most flapping wing micro air vehicles (FWMAV) are not capable of storing elastic energy [10][11]. Neither electric motors nor rigid body mechanisms that are typically used to drive the MAV can store elastic energy. In order to minimize the inertial power, several researchers have recently incorporated elastic energy storage in the motor-powered rigid-body mechanisms for flapping wings. Madangopal *et al* [12] showed in simulation that the inclusion of linear coil springs, which connect wing roots to the ground of a crank-rocker mechanism, can reduce the peak torque required from a motor as much as 12%, whereas Tantanawat and Kota [13] showed in simulation that it could reduce the peak input power as much as 42%. In practice, the additional spring adds extra payload but it does not mitigate friction loss that could be as substantial as wing inertial power. Baek and Fearing [14] showed experimentally that a wing flapper with a linear coil spring can only save the motor power above a threshold frequency, below which the friction loss dominates. Their measured power saving is up to 19%, which is smaller than the theoretical prediction by Ref. [13] .

Compliant mechanisms made of carbon-fiber reinforced polymer (CFRP) plates and polyimide film hinges are attractive for use to FWMAV because they are free of joint frictions and very lightweight [15][16][17]. If its polyimide film hinges could store enough elastic energy, the compliant mechanism could provide an effective solution to reduce energetic costs for FWMAVs. However, polyimide film hinges are generally soft and have not demonstrated sufficient elastic energy storage. Previously, extra springs were added to the polyimide-hinge compliant mechanism for elastic energy storage. In the example of a robot bee, a piezoelectric actuator served as an active spring coupled with the mechanism for elastic energy storage [15][16] [17][18]. In the example of a larger scale FWMAV (with <150mm wing span), a coil spring [14] or rubber strips [19] were added to the compliant mechanisms, which were driven by a motor. Recently, coil springs were also directly coupled with DC motors for direct drive of the flapping wings towards resonance[20][21][22].

It is not easy to design a polyimide-film-hinge compliant mechanism with sufficient elastic energy storage. If the film hinges are too soft, they will not store enough elastic energy. If they are too stiff, they will statically load more the motor and consequently reduce the dynamic wing stroke, just like stiff coil springs do to flapping wings[22]. Yet, inspiration can be drawn from Dipteran insects, which achieve both a large wing stroke and sufficient elastic energy storage. Dipteran insects quickly stop and subsequently reverse their wings through the interaction between wing bases and the thorax. There is a radial stop, i.e. a protrusion underside of wing base [23]. In the middle of a wing stroke where speed is maximal, the radial stop is idle and the wing hinges exhibit a low stiffness. Towards the end of a wing stroke, the radial stop is blocked by a tip of the elastic thorax, which exhibits increasing stiffness when increasingly deformed. Such non-linearly increasing stiffness exhibited over a quarter cycle of wing beat is believed

to be useful to design an energetically-efficient compliant mechanism for FWMAV.

In this paper, we shall present a lightweight compliant thoracic mechanism with polyimide hinges that can store elastic energy required for larger-size (10-15cm wing span) FWMAVs. As inspired by *Dipteran* flight thorax, this compliant mechanism is shaped as a shell structure, consisting of rigid plates and flexible hinges. Its activation for wing beating requires a nonlinearly increasing force towards the extreme wing stroke position. This compliant thoracic mechanism can store elastic energy comparable to the wings' inertial power up to a 25Hz wing beat frequency. We shall further show that power saving is effective only if elastic energy storage is well tuned to recover the inertial power.

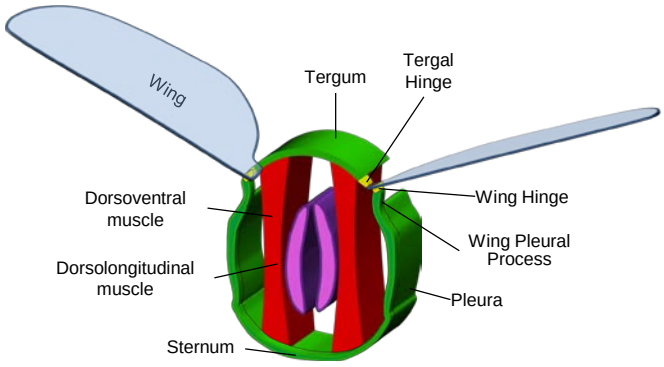

Fig. 1 Dipteran insect's flight thorax (After Snodgrass [24])

II. Thoracic Mechanism Design

A. Insect-inspired Design

The flight thorax segment of a Dipteran insect's exoskeleton is a deformable ring structure, onto which the wings are attached[3][25]. As shown in Fig. 1, the ring segment is composed of four joined rigid plates, namely a back plate (tergum), a belly plate (sternum), and two side plates (pleura). Among these plates, the sternum and pleura plates are rigidly joined while the tergum plate is movable relative to the rest. Wing bases are elastically hinged to the tergal and pleural plates. These exoskeleton plates are made of tough *chitin* lamellae (with Young's modulus of 7.848GPa[26]), while the wing hinges are composed of soft elastic *resilin* (with Young's modulus of 588.6kPa [26]). As the thorax is deformed by an agonist–antagonist muscles pair, the wings beat together with the reciprocating tergum plate. As mentioned, contact between the wing bases and the elastic thorax helps decelerate the wings towards the end of a wing stroke. Subsequently, the stored elastic energy in the thorax is released and helps to reverse the wings. In this way, the Dipteran insects save inertial power for flapping wings.

To address the need for elastic storage in a 10-15cm wing-span motorized FWMAV, we designed a compliant mechanism shaped like Dipteran insect's thorax. This thoracic mechanism is a deformable shell structure, made of CFRP exoskeleton plates and polyimide film hinges (Fig. 2). Fig. 3 shows that a symmetric half of the thoracic mechanism has a wing base plate elastically joined between a tergal plate and a pleural process plate. The pleural process plate is hinged to the anchor of pleural plate. Depression of the thorax at the tergal plate produces an upward wing stroke. Reversely, an upward tergal displacement produces a downward wing stroke. Reciprocation of the tergal plate is driven by a motor through a coupling crank-slider mechanism.

This compliant mechanism exhibits a nonlinearly increasing stiffness as its tergal plate is displaced from the neutral position towards the maximal position. Though configured differently, this thoracic mechanism can store elastic energy like that achieved by Dipteran insects through the interaction between the radial stop and elastic thorax. This geometrically nonlinear stiffness is attributed to plate rotations and elastic hinge deformations.

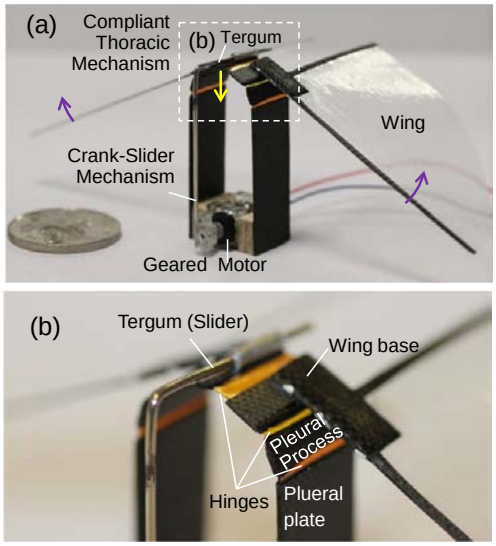

Fig. 2 Compliant thoracic mechanism with integrated polyimide film hinges for elastic energy storage. As the tergum of the thorax is depressed, its wings beat upwards.

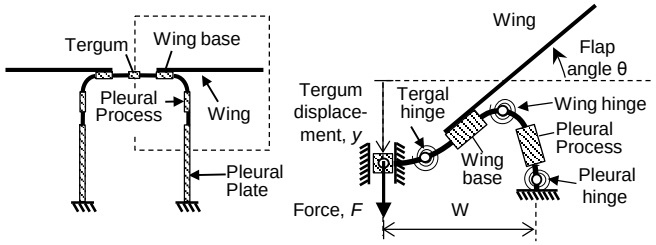

Fig. 3 A schematic drawing for the compliant thoracic mechanism: (left) a full thorax when not loaded; (right) a symmetric half thorax when it is loaded downward at its tergum plate.

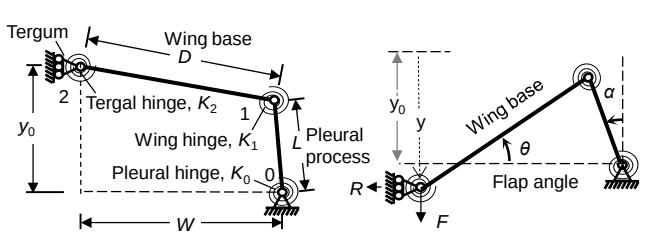

Fig. 4 A pseudo-rigid model for a symmetric half thorax: (left) neutral state when not loaded; (right) deformed state when the tergum (i.e. the slider) is loaded by a downward vertical force *F*.

B. Static Analysis

To simplify the geometrically nonlinear analysis, a symmetric half of the thoracic mechanism is modeled as a four-bar linkage with elastic torsional-springs in parallel with the joints. Fig. 4 shows this pseudo-rigid model: a slider representing the tergal plate while linkages of length D and L representing the wing base and pleural process plates respectively. Torsional springs at the joints represent polyimide hinges between the plates. The torsional stiffness of pleural hinge is K_0, while those for the wing and tergal hinges are K_1 and K_2 respectively. Torsional hinge stiffness can be calculated from the formula below, according to [27][28]:

$$K = \frac{dM}{d\theta} = \frac{EI}{H} \tag{1}$$

where E is the Young's Modulus, I is the beam cross-sectional area moment of inertia, and H is the equivalent hinge length.

This pseudo-rigid-model allows quick estimates for the wing rotation and the required force for a given tergal displacement. As such, the design of the thoracic mechanism can be iterated easily.

When not loaded, the tergum is statically positioned at the neutral point y_0, with the wing base angled slightly downward (see Fig. 4). As the tergum is depressed by a vertical force F downwards, the wing base plate rotates counterclockwise by an angle θ above the horizontal plane while the pleural process plate rotates by an angle α off the vertical plane. This causes a downward tergum displacement y off the neutral position:

$$y = y_0 + D\sin\theta - L\cos\alpha \tag{2}$$

As the anchor to the pleural wall has a constant distance W from the plane of symmetry, the rotations of wing-base and pleural-process plates will satisfy the following constraint:

$$W = D\cos\theta + L\sin\alpha \tag{3}$$

Equations (2) and (3) suggest that the wing stroke angle per tergum displacement depends on the linkage lengths D and L.

The depressive force F on the tergum is resisted by the spring forces of the thoracic compliant mechanism. It can be determined from a force analysis of the individual linkages. The moment equilibrium for the pleural process plate yields:

$$K_0\alpha + K_1\left(\theta - \alpha + \frac{\pi}{2}\right) - FL\sin\alpha + RL\cos\alpha = 0 \tag{4}$$

The moment equilibrium for the wing base plate yields:

$$K_1\left(\theta - \alpha + \frac{\pi}{2}\right) + K_2(\theta) - FD\cos\theta - RD\sin\theta = 0 \tag{5}$$

The force acting on the tergum plate is determined as a function of the joint angles following:

$$F = \frac{\left\{K_0\alpha + \left[K_1\left(\theta - \alpha + \frac{\pi}{2}\right)\right]\left(1 + \frac{L\cos\alpha}{D\sin\theta}\right) + K_2(\theta)\frac{L\cos\alpha}{D\sin\theta}\right\}}{L\left(\sin\alpha + \frac{\cos\alpha\cos\theta}{\sin\theta}\right)} \tag{6}$$

The force increases with the increasing tergum displacement from the neural position. As the thoracic mechanism is deformed, the elastic energy stored in it is equal to the work done by the depressive force F on the tergum plate. Integration of the force over the tergal displacement y yields:

$$W_{elastic} = \int_0^{y_{max}} F dy \tag{7}$$

in which F and y are functions of θ according to Eqs. (2) and (6) respectively. The maximum elastic storage depends on the maximal tergal displacement y_{max}, which is determined by the crank length of a motorized crank-slider mechanism.

In a quarter cycle of the wing stroke as the thorax is depressed, the applied force is in the direction of the tergum displacement. This results in elastic energy storage in the flexures of the thorax. In the next quarter cycle as the thorax is relaxed, the stored elastic energy is released and converted into wing kinetic energy. Similarly, the energy storage and release happen as the tergum of the thorax is lifted.

C. Design and Elastic Properties

A thoracic compliant mechanism is designed with the listed parameters in Table 1. For simplicity, its wing base D is designed to be the same as the spacing W between the pleura anchor and the symmetry plane. Among the three elastic hinges in a half thorax, the wing hinge between the wing-base and pleural-process plates is designed with the least stiffness K_1 to allow for a large wing stroke. The tergal hinge between the tergum and wing-base plates is stiffer at K_2 to transfer the actuation force. The pleural hinge between the pleural-process plate and the anchor is the stiffest at K_0 to store the most elastic energy. These hinges will be bent most towards the maximal tergal displacement, up or down.

This design intends to produce a static wing stroke of 60° given ±3mm of tergum displacement, when driven by a 6-mm diameter coreless DC gearmotor (Precision Microdrives 206-102[29]) through a 3mm long crank.

Table 1 Parametric values for the pseudo rigid model.

Parameter	Input Value
D	7 mm
W	7 mm
L	4 mm
K_0	4.267 mNm/rad
K_1	0.03414 mNm/rad
K_2	0.1366 mNm/rad

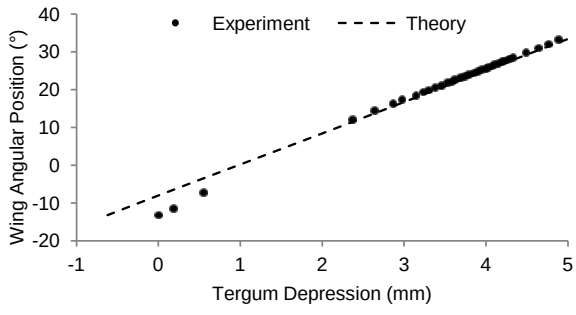

Fig. 5 Wing angular position as a function of tergum depression of the compliant mechanism.

To measure its elastic properties, the thorax was statically loaded with increasing deadweights at a 1-gram increment and photographs of its deformed shapes were taken in sequence. This thoracic design is observed from Fig. 5 to sweep a 10° wing stroke for a 1 mm tergal displacement. Meanwhile, the force acting on the tergum increases non-linearly with the

tergum displacement as shown in Fig. 6. The elastic energy stored in the thorax can be calculated from the area under the force-displacement curve. It amounts to 0.4937mJ at a 4.20 mm tergum displacement (i.e. at a 33.2° wing stroke). As shown in these figures, the analytical estimates agree well with measurements.

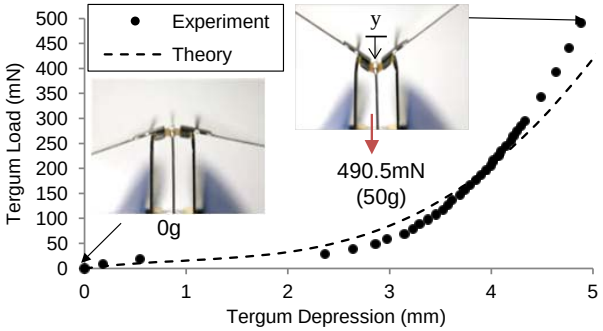

Fig. 6 The static force required to depress the tergum plate of the compliant thoracic mechanism.

III. Fabrication of the Transmission Mechanism

A. *Compliant Thoracic Mechanism*

This thoracic mechanism is a deformable shell structure made of CFRP plates and polyimide film hinges. CFRP plates and polyimide hinges can be fabricated and integrated on a strip of polyimide film (DuPont Kapton HN) by selective reinforcement [30][31][32]. Plates are CFRP reinforced patches while a hinge is an unreinforced film spacing between the reinforced patches. The CFRP patches were obtained by manual cutting CFRP prepreg (HexPly M10R/38%/UD150/ CHS) using a rotary blade cutter. For this thoracic mechanism design, the three hinges of distinct stiffness were made from three separate polyimide strips of different film thickness as shown in Fig. 7.

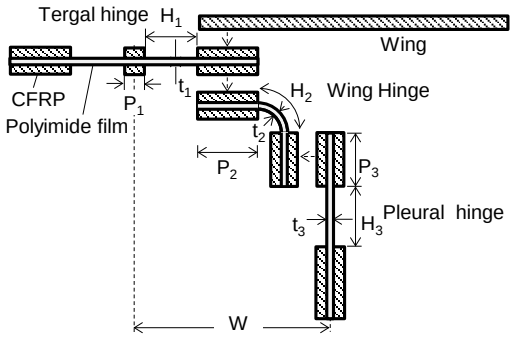

Fig. 7 Assembly of a half compliant thoracic mechanism from three strips of polyimide hinge/CFRP plates.

As listed in Table 2, film hinges were prepared from 10 mm wide polyimide films of distinct thickness: 50.8μm thick tergal hinge, 25.4μm thick wing hinge, and 127.0 μm thick pleural hinge. After selectively reinforced by CFRP patches, the three strips of integrated hinge and plates were assembled by lapping and adhesively bonding over common plate areas. The assembly were subsequently folded and mounted to an acrylic plate housing. As a result of these fabrication processes and assembly, the thoracic compliant mechanism was obtained as shown in Fig. 2.

This wing design adopts a semi-elliptical shape, which has a 50 mm long leading edge and a 31 mm long root chord. The leading edge of the wing foil is reinforced spanwise by CFRP on both sides; whereas, the root chord of the wing foil is lightly reinforced with one-side CFRP such that it is flexible chord-wise for passive wing rotation about the leading edge. Table 3 lists and compares this transmission mechanism and wing properties with a rigid-body mechanism described next.

Table 2 Design parameters of the polyimide hinges

Design Part	Symbol	Dimension
Tergal hinge	t_1	0.0508 mm
	H_1	2 mm
	P_1	1 mm
Wing hinge	t_2	0.0254 mm
	H_2	1 mm
	P_2	3 mm
Pleural hinge	t_3	0.1270 mm
	H_3	1 mm
	P_3	2.5 mm
Width for film hinges		10 mm
Half space between pleura	W	7 mm

B. *Benchmark Rigid Body Mechanism*

To serve as a benchmark for comparison, a rigid-body mechanism was developed to bear the same wings and beat almost the same wing kinematics (80° wing stroke) as the compliant thoracic mechanism does. This rigid-body mechanism is an assembly of acrylic linkages, and revolute and prismatic joints, and metal pins. These linkages and its joints or slots were fabricated by laser cutting 1 mm thick acrylic plates.

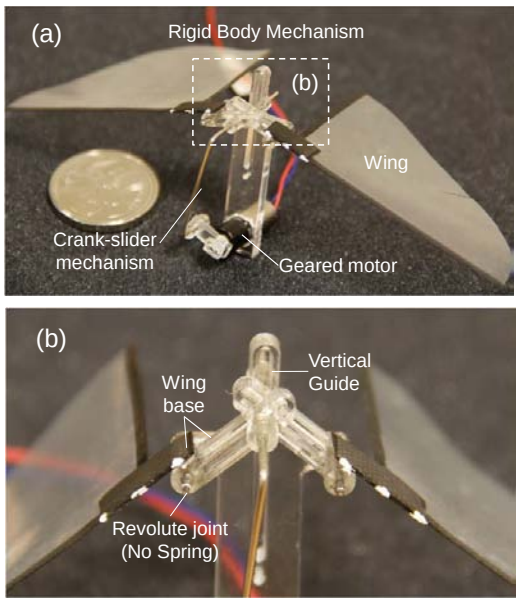

Fig. 8 A benchmark flapping-wing rigid body mechanism without capability for elastic energy storage.

As shown in Fig. 9, this rigid-body mechanism has a pair of wing levers. The proximal end of each wing lever is a pivoted guide (i.e. wing base) about a fulcrum, which is spaced from the other fulcrum at a distance 2*W*, the same as the pleural wall spacing for the compliant mechanism. Wing bases of the two wing levers are coupled with a pin and guided vertically. As the pin is reciprocated by a motor-powered crank slider mechanism, each wing base is driven into angular oscillation about each fulcrum. Each of the wing bases (i.e. the plastic guides) weighs 0.08g and contributes very little rotational inertia, at 2.69gmm^2 as compared to 72.05 gmm^2 of each wing. To minimize the friction loss between its pin and guides, the rigid-body mechanism is lubricated with oil.

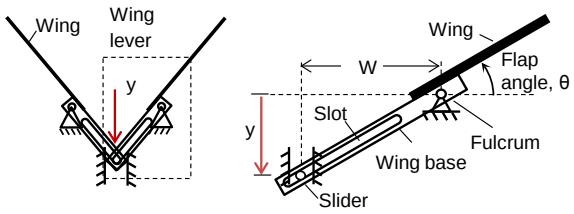

Fig. 9 Schematic design of the rigid-body mechanism, which consists of a pair of wing levers coupled with a slider that reciprocates with motion in the y-direction.

Table 3 Design specifications for the compliant thoracic mechanism and rigid body benchmark mechanism.

Design specifications	Compliant Mechanism	Rigid Body Mechanism
Dynamic (Static) wing stroke	79° (56°)	85° (80°)
Wing span (tip to tip)	100mm	100mm
Wing rotational inertia, J_0	7.21×10^{-8}kgm^2	7.21×10^{-8}kgm^2
Half space between pleura, *W*	7mm	7mm
Crank length	3mm	5mm
Weight	3.51g	3.34g

IV. Energetic Costs Analysis

While performing flapping-wing flight, a micro air vehicle expends substantial power to move its wings through the air. Internal to the vehicle, additional power is required to overcome friction loss and elastic loads in its mechanism. Hence, the total mechanical power (P_{mech}) generated by a primary driver, i.e. the electric motor, is equal to the sum of the aerodynamic power (P_{aero}), the wings' inertial power ($P_{inertia}$), the elastic power ($P_{elastic}$), and the friction loss (P_{losses}), as follow:

$$P_{mech} = P_{aero} + (P_{inertia} + P_{elastic}) + P_{losses} \quad (8)$$

Ideally, one could design an elastic element to fully recover the wing kinetic energy, which would otherwise be wasted without the elastic energy storage mechanism. An elastic element in the mechanism seemingly poses additional load to the motor. However, the elastic element does not draw a net power over a cycle of the wing motion. Indeed, it helps to convert the wing's kinetic energy into elastic strain energy in a quarter cycle and to release the stored elastic energy for wing reversal in the subsequent quarter cycle.

As the sum of kinetic and elastic energies of the flapping-wing mechanism is conservative, their time derivative should vanish following Rayleigh's energy method[33]. Therefore, the sum of inertial and elastic power would vanish:

$$P_{inertial} + P_{elastic} = 0 \quad (9)$$

As a result, the average mechanical power reduces to only the dissipative powers:

$$P_{mech} = P_{aero} + P_{losses} \quad (10)$$

This suggests that the elastic energy storage could help reduce the motor's electrical power and torque required to drive flapping-wing flight. However, if the elastic energy storage is not sufficient to fully recover the wings' kinetic energy, the sum of the inertial and elastic powers will not be reduced to zero.

In measurement, the averaged inertial and elastic power can be estimated semi-analytically from the measured wing kinematics and static elastic storage capacity.

The average inertial power can be estimated from the maximum change of wing kinetic energy over a quarter cycle of the wing beat, where the speed peaks at the mid-stroke [4] [5]:

$$\bar{P}_{inertial} = 4\pi^2\phi^2 f^3 J_0, \quad (11)$$

where f is the wing beat frequency, ϕ is the wing stroke angle, and J_0 is the rotational inertia of each wing. This estimate assumes that the wing stroke profile is a sinusoidal function of time and the maximum angular speed of the wing beat is $\pi f\phi$.

On the other hand, the averaged elastic power can be estimated from the maximum elastic energy storage over a quarter cycle of the wing beat as the elastic elements are stopping the wings:

$$\bar{P}_{elastic} = -4fW_{elastic} \quad (12)$$

in which $W_{elastic}$ is the work done on the elastic element as derived in Eq. (7).

The input mechanical power to the flapping-wing mechanism is generated by the electric motor, which runs at the same frequency f as the wing beat frequency. It can thus be calculated as the product of motor torque and motor speed:

$$\bar{P}_{mech} = 2\pi f k_m \bar{I}, \quad (13)$$

in which $2\pi f$ is the motor speed, k_m is the motor torque constant (7.664mNm/A), and $\bar{I}$ is the average current drawn by the motor (Precision Microdrives 206-102 [29]). The time-varying current to drive the motor at a constant voltage can be accurately measured using a precision source/measure unit (Agilent B2902A). Motor efficiency can be calculated by comparing this output mechanical power with the input electrical power.

V. Experiment, Results and Discussions

The compliant thoracic mechanism can store elastic energy, whereas the rigid body mechanism cannot. To isolate the effect of elastic storage on energetic costs, the two mechanisms are designed to beat the same wings with approximately the same wing kinematics. In this way, any power saving by the compliant mechanism to produce the same thrust could provide a measure for the effectiveness of the elastic energy storage.

A. *Wing Kinematics and Thrust*

In a lightly damped free vibration test, this winged thoracic compliant mechanism exhibits a natural frequency over a range of 30~37Hz, depending on the crank position. Fig. 10 shows free oscillation of a wing attached on the thoracic compliant mechanism whose tergum is cranked up. As the thorax is driven by a motor into forced oscillation, its dynamic wing stroke increases with increasing wing beat frequency. Fig. 11 shows that the wing stroke angle increased from a static angle of 55° at 0Hz to a higher dynamic angle of 78° at 25 Hz. This 42% enhancement of the dynamic wing stroke angle is attributed to hinge flexibility and reduced dynamic stiffness of the thorax. Due to the added virtual mass of air trapped by flapping wings [34][35], its resonance for the forced oscillation is expected to occur at a lower driving frequency than the natural frequency. However, resonance peak is not observed from Fig. 11 due to increasing loads with higher frequency.

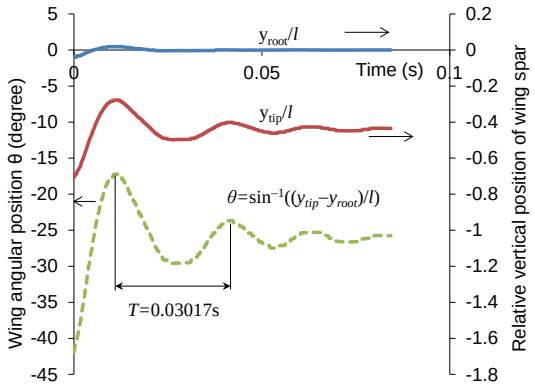

Fig. 10 Free oscillation of a wing about its root which was supported on a compliant thoracic mechanism whose tergum was cranked up. Wing spar positions, at the tip (y_{tip}) and the root (y_{root}) between which were spaced at length (l), were tracked from a high-speed video of the oscillation.

In comparison, the wing stroke angle generated by the rigid-body mechanism is not frequency dependent. It remains nearly constant at 85°, slightly above the static angle of 80°, throughout the whole frequency range. Above 22 Hz, both compliant and rigid-body mechanisms generate almost the same wing stroke angle. For example, Fig. 12 shows a cycle of wing beat of similar wing stroke amplitude at 25Hz for the two mechanisms. In addition, it is noted from Fig. 11 that the maximum driving frequency for either mechanism is limited by the motor capacity. However, a lower driving voltage is required for driving the compliant mechanism, as compared to that driving the rigid-body mechanism at the same wing beat frequency (see Fig. 12).

Thrust generated by the wing flappers can be measured on a tethered flight test stand using a simple pendulum method [36][37]. As shown in Fig. 13, the wing flapper was attached at the distal end of the pendulum rod, which pointed vertically downward under gravity when the flapper was idle. As wings flaps, thrust is generated to raise the pendulum (i.e. the rod and the flapper) by a quasi-static angle off the vertical line. The quasi-static angle is a result of the moment equilibrium between the gravity and thrust. It provides a measure for the thrust, as long as the pendulum and flappers were not raised above the horizontal line.

This tethered flight test demonstrated that the thrust generated by the wing flappers increases with the increasing wing beat frequency (see Fig. 14). Meanwhile, the thrust generated by the compliant depends also on the dynamic wing stroke, which varies with the frequency. Over the low driving frequency range, the compliant mechanism produces less thrust than the rigid-body mechanism does, e.g. at most 18% lower at 15 Hz, due to a smaller wing stroke. However, this thrust difference appears small in the plot along with much larger thrust magnitude at higher frequencies. Over the higher frequency range above 25 Hz, the thrust generated by the compliant mechanism increases and become almost equal to the thrust generated by the rigid-body mechanism as its dynamic wing stroke increases as much as that of rigid-body mechanism. As such, the effect of elastic energy storage can be better seen by comparing their energy energetic costs over the high frequencies.

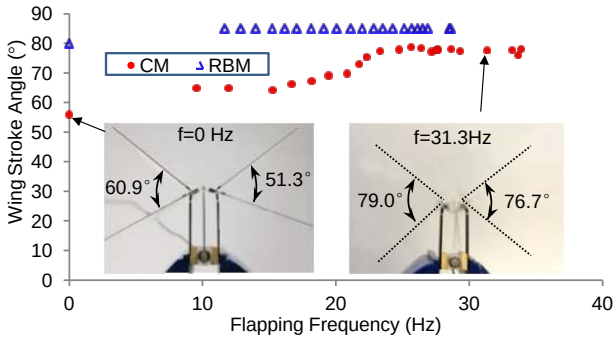

Fig. 11 Wing stroke angles for the compliant mechanism (CM) and rigid body mechanism (RBM) as a function of the wing beat frequency.

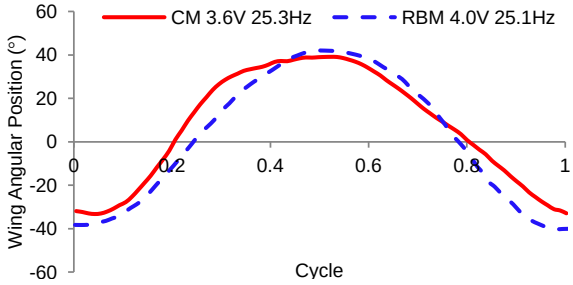

Fig. 12 Wing stroke position as a function of time over one wing beat cycle at approximately 25 Hz.

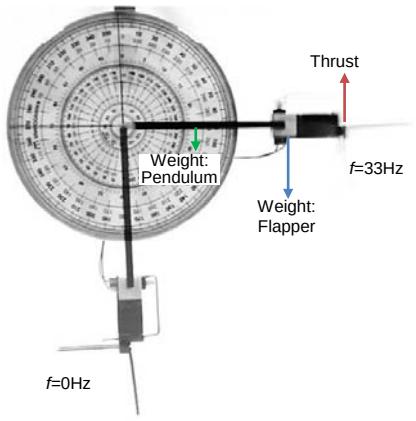

Fig. 13 Tethered flight test using a simple pendulum: When the wing flapper at the pendulum's end was idle, the pendulum pointed downward under the gravity; when the wing flappers beat at 33 Hz, the pendulum of wing flappers was lifted above the horizon by the generated thrust.

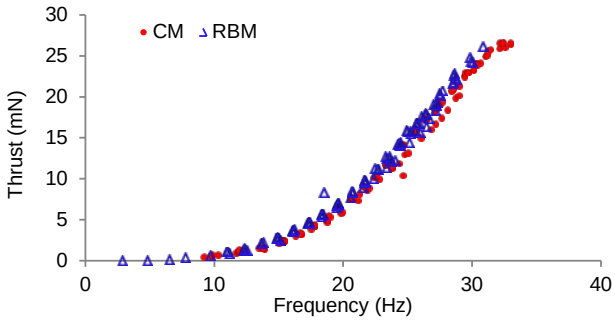

Fig. 14 Thrust generated by the flapping-wing compliant and rigid-body mechanism as a function of the wing beat frequency.

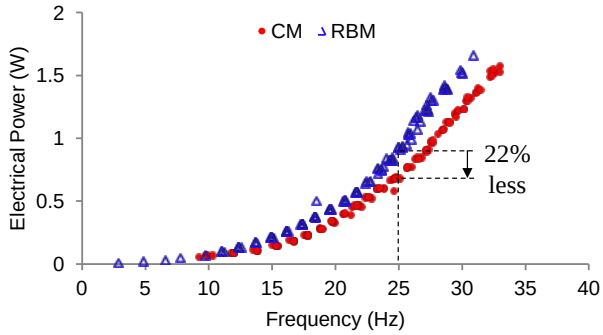

Fig. 15 The average electrical power required by the same motor to drive the compliant and rigid-body mechanisms as a function of wing beat frequency. The average electrical power required to drive the compliant mechanism is less than that required to drive the rigid body mechanism.

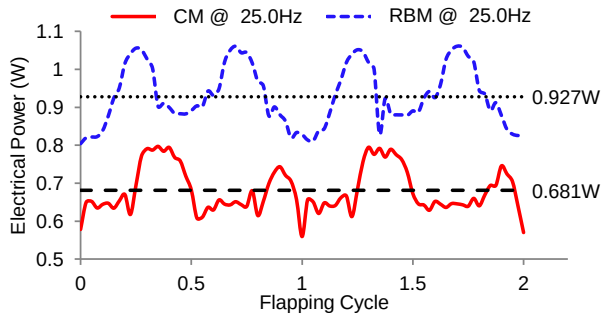

Fig. 16 Electrical powers required to drive the compliant and rigid-body mechanisms over two wing beat cycles at 25 Hz. The average power required to drive the compliant mechanism (CM) is lower than that required to drive the rigid body mechanism (RBM).

B. Reduced Energetic Cost

The electrical power required by a DC motor to drive flapping wings depends on several factors, namely wing beat frequency, aerodynamic load, and mechanism design. Meanwhile, the aerodynamic load increases with the wing stroke and wing beat frequency. Fig. 15 shows that the average electrical power required increases with the wing beat frequency. It is noted that the motor driving the compliant mechanism consumes less electrical power than that driving the rigid-body mechanism. For example, the compliant mechanism consumes 31% less power while beating wings at 15Hz. It consumes 22% less power while beating wings at 25Hz. During a cycle of wing beat, the motor powers are observed from Fig. 16 to peak twice towards the ends of wing strokes, either up or down.

To better isolate the effect of elastic energy storage, one can alternatively compare the two mechanisms in term of the thrust-to-power ratio, which measures the effectiveness of the mechanism to convert electrical power to aerodynamic thrust using the same motor. Fig. 17 shows that, for either mechanism, the generated thrust per power increases at decreasing rates with the increasing frequency, up to an 'optimum' frequency beyond which the effectiveness drops. Instead of the influence by elastic resonance, the drop of thrust per power beyond the maximum is believed to be attributed to limited motor capacity. This belief is supported by Fig. 18 showing that the motor efficiency decreases with faster flapping, which loads more either mechanism. Due to the reduced reactive load, the motor efficiency is improved by using the compliant mechanism, instead of the rigid-body mechanism. As a result, the compliant mechanism produces more thrust per power than the rigid-body mechanism over the same to frequency, e.g. 20% more at 25Hz.

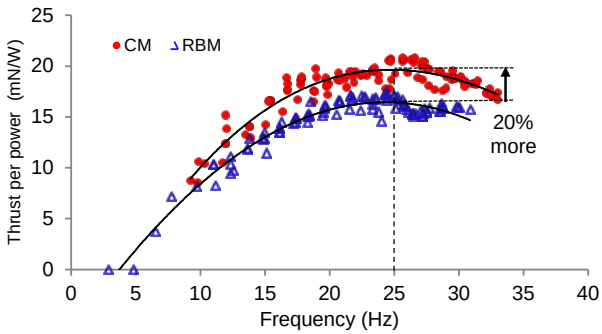

Fig. 17 Thrust to electrical power ratio (T/P) achieved by the compliant and rigid-body mechanisms. Over the frequency range from 15Hz to 30Hz, the compliant mechanism (CM) produces 19-22% more thrust per unit power as compared to the rigid-body mechanism (RBM).

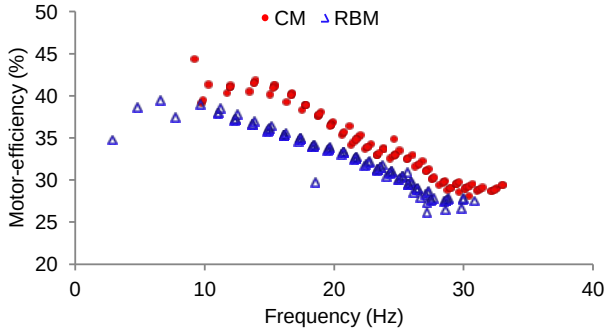

Fig. 18 Motor mechanical efficiency to convert electrical power to mechanical power.

C. Power Components Over Frequency

To verify if sufficient elastic energy storage could fully recover the wing inertial power following Eq. 9, we shall analyze the breakdown of the power components which are consumed by each flapping-wing mechanism.

Mechanical power measurement provides a means to indirectly measure a power component, which differs in two distinct operating conditions. For example, the mechanical power incurred to drive a wing flapper in air ($\bar{P}_{mech}$) is higher

than that in vacuum ($\bar{P}_{mech,vac}$) due to the absence of aerodynamic power ($\bar{P}_{aero}$) in vacuum[10][11]. On the other hand, the mechanical power required to drive a wingless flapper in air ($\bar{P}_{mech,wingless}$) is mainly due to the friction loss of the gears and motor shaft ($\bar{P}_{losses}$). Hence, the apparent inertial power ($P_{inertial} + P_{elastic}$) can be estimated as the difference between the mechanical power for driving winged mechanism in vacuum and that for driving the wingless mechanism, which was tested in air instead of vacuum to avoid motor overheating.

Fig. 19 shows the mechanical powers required to drive the compliant mechanism under various conditions while Fig. 20 shows the power required to drive the rigid-body mechanism under those conditions. In general, the mechanical power required increased with the wing beat frequency. Interestingly, it is observed from Fig. 21 that the apparent inertial power for the compliant mechanism vanishes over the frequency range up to 25Hz. In contrast, the inertial power for the rigid-body mechanism remains substantial and increases monotonically with increasing frequency. However, beyond 25 Hz, the compliant mechanism cannot fully recover the inertial power because the wing inertial power then exceeds the elastic power capacity as shown in Fig. 22.

To this thoracic compliant mechanism with nonlinear stiffness, the effect of resonance is not obvious in reducing the electrical power (see Fig. 15), unlike how it did to the linear elastic system [21][22]. However, sufficient elastic energy storage, even by a nonlinear one, is effective to reduce the inertial power. For example, to drive a compliant mechanism at 25 Hz, the inertial power amounts to merely 2% of the total power (see Fig. 19). On the other hand, to drive a rigid-body mechanism at the same frequency of 25 Hz, the inertial power amounts to 23% of the total mechanical power (see Fig. 20). The inertial power remains low up to 25Hz wing beat frequency and it dips slightly with increasing frequency towards 25 Hz (see Fig. 21).

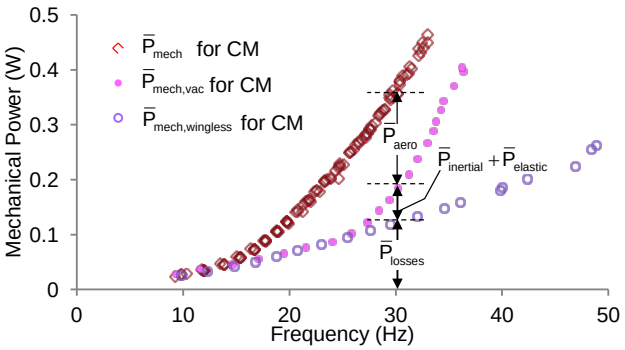

Fig. 19 Mechanical power required to drive the compliant thoracic mechanism under different operating conditions.

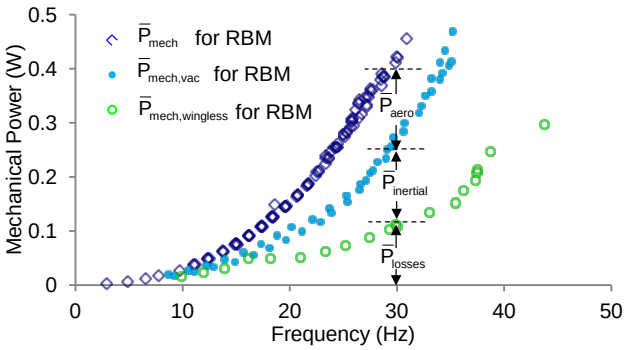

Fig. 20 Mechanical power required to drive the rigid body mechanism under different operating conditions.

D. Comparison with Previous Works

In comparison with coil springs (as listed in Table 4), polyimide film hinges are much lighter in weight. The CFRP shell structure with these integrated polyimide film hinges exhibit nonlinear increasing stiffness as its tergum plate is depressed increasingly. This shell structure exhibited a low stiffness when it is at the neutral position, where the wing speed reaches maximum; whereas, it exhibits high stiffness, up to 700 N/m when it reaches its maximum position where the wing stroke is stopped. As such, it stores sufficient elastic energy storage, without loading the motor unnecessarily near the neutral position. As a result, this thoracic compliant mechanism is effective for fully recovering the inertial power from a low wing beat frequency up to 25 Hz. In contrast, the previous compliant mechanism with a discrete linear spring[14] could only save power above a 15Hz frequency threshold, which is about 66% of the 24.5 Hz resonant frequency. In a recent work, coil springs were directly coupled with DC motor for flapping wings [22][40], but information of power saving by adding springs were not available for comparison.

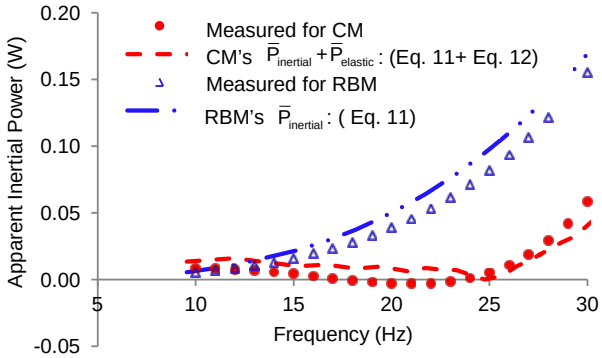

Fig. 21 Apparent inertial powers requirement for the compliant mechanism and the rigid-body mechanism as a function of wing beat frequency. Semi-analytical estimates were calculated from Eqs. 11 and 12.

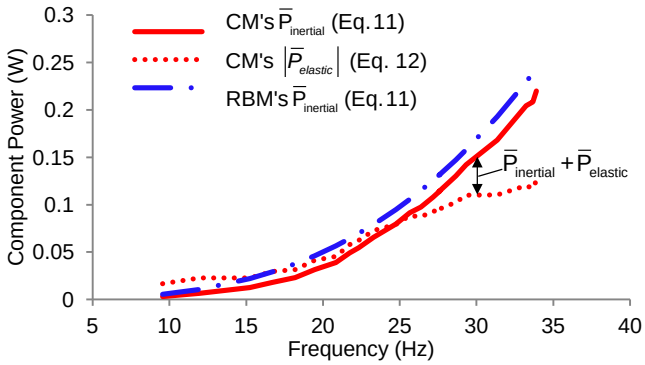

Fig. 22 Calculated inertial powers and elastic power as a function of wing beat frequency, following Eqs. 11 and 12 respectively and using the measured wing stroke and wing beat frequency.

Table 4 Comparison among various flapping-wing mechanisms with capability of elastic energy storage

Current and Previous Works	MAV Weight	Wing Span	Wing stroke	Flapping Frequency	Spring Type	Spring Stiffness	Spring Weight	Power Saving
This thoracic compliant mechanism	3.51g	100mm	56°-80°	9-33Hz	Shell Structure	0-700N/m	0.066g	31% max
Baek's compliant mechanism[14]	5.8g	80mm [a]	~55°	10-30 Hz	Coil Spring	140N/m	0.259g [b]	30% max
Vamp RC (rigid-body mechanism)[14]	13.0g	304.8mm	45°	16Hz	Coil Spring	980N/m	0.444g [c]	19% max
Sahai's compliant mechanism[19] [38]	3.0g	124mm	100°	16-18Hz	Rubber Strips	3.2mNm/rad	0.02g	20% max
Bejgerowski's compliant mechanism[39]	12.76g	152mm	65°	12.1Hz	Leaf springs	0.7mNm/deg	–	–
Madangopal's rigid-body mechanism [12]	–	600mm	90°	0.8Hz	Coil Spring	51.3N/m	–	(12% torque)
Tantanawat's rigid-body mechanism[13]	–	660mm	44.8°	4Hz	Coil Spring	38N/m	–	42% predicted
Hines' Direct Motor-Driven Flapping [22]	2.7g	140mm	40-160°	2-20Hz	Coil Spring	2.83mNm/rad	0.12g [d]	-
Roll's Electromagnetic Actuator[40][41]	5.2g [e]	90-140mm	68-107°	30-71Hz	Magnet	0-5.64mNm/rad	-	-

[a] Estimated from the scale of photo image

[b] Estimated for a 5.5mm-diameter coil spring with 10 turns, made of a bronze wire of 0.44mm diameter and spring free length of 21.5mm. The phosphorous bronze Grad A has a Young modulus of 103GPa, and a density 8860kg/m3

[c] Estimated for a 5.5mm-diameter coil spring with 8 turns, made of a bronze wire of 0.65mm diameter and spring free length of 21.5mm.

[d] Estimated by the difference between the wing-motor mass and the total system mass.

[e] Estimated based on two actuators each with a single wing.

VI. Conclusions

We have presented a compliant thoracic mechanism with integrated polyimide film hinges for elastic energy storage. These film hinges add no almost extra weight to the compliant mechanism, which consists of CFRP plates and polyimide film. Due to hinge flexibility, this thoracic compliant mechanism enhances the dynamic wing stroke angle up to 42% higher than the static wing stroke angle when beating wings above 22Hz frequency. As a closed-form shell structure, this compliant thoracic mechanism exhibited nonlinear stiffness characteristics, with increasing stiffness from a low value at the neutral position to as much as 700N/m at the maximal position. As a result, it can provide sufficient elastic storage to fully recover the kinetic energy from 100-mm-span wings flapping at 25Hz. This power saving is attributed to almost zero apparent inertial power, which is verified both experimentally and theoretically, with sufficient elastic energy storage. In future, we shall further investigate the effectiveness of such means of elastic energy storage for a larger flapping-wing micro air vehicles (with greater-than-240-mm wing span), which could carry more payload.

Acknowledgement

This work is with financial support by the Defense Science and Technology Agency (DSTA) of Singapore through Defense Innovation Research Program (DIRP). The second author is grateful to Nanyang Technological University for the award of graduate scholarship to support his graduate study.

References

[1] U. M. Norberg, T. H. Kunz, J. F. Steffensen, Y. Winter and O. V. Helversen, "The Cost of Hovering and Forward Flight in a Nectar-Feeding Bat, Glossophaga Soricina, Estimated from Aerodynamic Theory," *Journal of Experimental Biology,* vol. 182, pp. 207-227, 1993.

[2] T. Weis-Fogh, "Energetics of Hovering Flight in Hummingbirds and in Drosophila," *Journal of Experimental Biology,* vol. 56, pp. 79-104, 1972.

[3] R. F. Chapman, The Insects: Structure and Function, 4th ed., Cambridge: Cambridge University Press, 1998.

[4] C. P. Ellington, "The Aerodynamics of Hovering Insect Flight. VI Lift and Power Requirements," *Philosophical Transactions of the Royal Society of London. B,* vol. 305, no. 1122, pp. 145-181, 1984.

[5] C. v. D. Berg and J. M. V. Rayner, "The Moment of Inertia of Bird Wings and The Inertial Power Requirement for Flapping Flight," *Journal of Experimental Biology,* vol. 198, pp. 1655-1664, 1995.

[6] C. Ellington, "Power and Efficiency of Insect Flight Muscle," *Journal of Experimental Biology,* vol. 115, pp. 293-304, 1985.

[7] T. Weis-Fogh, "Quick Estimates of Flight Fitness in Hovering Animals, Including Novel Mechanism for Lift Porduction," *Journal of Experimental Biology,* vol. 59, pp. 169-230, 1973.

[8] R. M. Alexander and H. C. Bennet-Clark, "Storage of elastic strain energy in muscle and other tissues," *Nature,* vol. 265, pp. 114-117, January 1977.

[9] M. H. Dickinson, "Muscle Efficiency and Elastic Storage in the Flight Motor of Drosophila," *Science,* vol. 268, no. 5207, pp. 87-90, 7 April 1995.

[10] D. Lentink, S. Jongerius and N. Bradshaw, "The scalable design of flapping micro air vehicles inspired by insect flight," in *Flying insects and robots,* Springer-Verlag Berlin Heidelberg, 2009, pp. 185-205.

[11] M. Keennon, K. Klingebiel, H. Won and A. Andriukov, "Development of the Nano Hummingbird: A Tailless Flapping Wing Micro Air Vehicle," in *60th AIAA Aerospace Sciences Meeting Including the New Horizons Forum and Aerospace Exposition*, Nashville, Tennessee, 9-12 January 2012.

[12] R. Madangopal, Z. A. Khan and S. K. Agrawal, "Biologically Inspired Design Of Small Flapping Wing Air Vehicles Using Four-bar Mechanisms and Quasi-steady Aerodynamics," *Journal of Mechanical Design*, vol. 127, no. 4, pp. 809-816, 2005.

[13] T. Tantanawat and S. Kota, "Design of Compliant Mechanisms for Minimizing Input Power in Dynamic Applications," *Journal of Mechanical Design,* vol. 129, no. 10, pp. 1064-1075, 2007.

[14] S. S. Baek, K. Y. Ma and R. S. Fearing, "Efficient Resonant Drive of Flapping-Wing Robots," in *The 2009 IEEE/RSJ International Conference on Intelligent Robots and Systems*, St. Louis, USA, 2009.

[15] A. Cox, D. Monopoli, D. Cveticanin and M. Goldfarb, "The Development of Elastodynamic Components for Piezoelectrically Actuated Flapping Micro-air Vehicles," *Journal of Intelligent Material Systems and Structures*, vol. 13, pp. 611-615, 2002.

[16] M. Sitti, D. Campolo, J. Yan and R. S. Fearing, "Development of PZT and PZN-PT Based Unimorph Actuators for Micromechanical Flapping

Mechanisms," in *IEEE International Conference on Robotics and Automation (ICRA)*, 2001.

[17] R. Wood, "Liftoff of a 60mg flapping-wing MAV," in *2007 IEEE/RSJ International Conference on Intelligent Robots and Systems*, San Diego, CA, USA, 2007.

[18] V. Arabagi, L. Hines and M. Sitti, "Design and manufacturing of a controllable miniature flapping wing robotic platform," *The International Journal of Robotics Research*, vol. 31, no. 6, pp. 785--800, 2012.

[19] R. Sahai, K. C. Galloway and R. J. Wood, "Elastic Element Integration for Improved Flapping-Wing Micro Air Vehicle Performance," *IEEE Transactions on Robotics*, vol. 29, no. 1, pp. 32-41, 2013.

[20] M. Azhar, D. Campolo, G. K. Lau, L. Hines and M. Sitti, "Flapping wings via direct-driving by DC motors," in *2013 IEEE International Conference on Robotics and Automation (ICRA)*, 2013.

[21] D. Campolo, M. Azhar, G. K. Lau and M. Sitti, "Can DC motors directly drive flapping wings at high frequency and large wing strokes?," *IEEE/ASME Transactions on Mechatronics, (Volume:19 , Issue: 1)* , vol. 19, no. 1, pp. 109 - 120 , 2014.

[22] L. Hines, D. Campolo and M. Sitti, "Liftoff of a Motor-driven, Flapping Wing Micro Aerial Vehicle Capable of Resonance," *IEEE Transactions on Robotics*, vol. 30, no. 1, pp. 220-232, 2014.

[23] A. R. Ennos, "A Comparative Study of The Flight Mechanism of Diptera," *Journal of Experimental Biology*, vol. 127, pp. 355-372, 1987.

[24] R. Snodgrass, Principles of Insect Morphology, New York: McGraw-Hill Book Co., 1935.

[25] P. J. Gullan and P. S. Cranston, The Insects: An Outline of Entomology 4th Ed, Wiley-Blackwell, 2010.

[26] M. Jensen and T. Weis-Fogh, "Biology and Physics of Locust Flight. V. Strength and Elasticity of Locust Cuticle," *Philosophical Transactions of the Royal Society of London. Series B, Biological Sciences*, vol. 245, no. 721, pp. 137-169, 1962.

[27] L. L. Howell, Compliant Mechanisms, New York: John Wiley & Sons, Inc, 2001.

[28] G. K. Lau, H. T. Lim, J. Y. Teo and Y. W. and Chin, "Lightweight mechanical amplifiers for rolled dielectric elastomer actuators and their integration with bio-inspired wing flappers," *Smart Materials and Structures*, vol. 23, no. 2, p. 025021, 2014.

[29] Website, "Product Data Sheet Nano Planetary™ 6mm DC Gearmotor - 16mm Type," Precision Microdrives Limited, 2014. [Online]. Available: https://catalog.precisionmicrodrives.com/order-parts/.

[30] R. J. Wood, S. Avadhanula, R. Sahai, E. Steltz and R. Fearing, "Microrobot design using fiber reinforced composites," *Journal of Mechanical Design*, vol. 130, p. 052304, 2008.

[31] W. X. Teo, G. K. Lau and H. K. H. Li, "Bio-inspired thorax for flapping-wing robotfly," *Proc. of SPIE Vol. 7643*, p. 76431P, 2010.

[32] Y. W. Chin and G. K. Lau, ""“Clicking” compliant mechanism for flapping-wing micro aerial vehicle," in *2012 IEEE/RSJ International Conference on Intelligent Robots and Systems (IROS),*, 2012.

[33] R. F. Steidel, "Chapter Three: Energy Methods," in *An Introduction to Mechanical Vibrations*, John Wiley & Sons, 1989, pp. 71-72.

[34] R. Dudley, "3.2.2.1 Virtual Mass Forces," in *The Biomechanics of Insect Flight: Form, Function*, Princeton University Press, 1999, pp. 126-127.

[35] R. J. Wood, "Design, fabrication, and analysis of a 3DOF, 3cm flapping-wing MAV," *IEEE/RSJ International Conference on Intelligent Robots and Systems (IROS 2007)*, pp. 1576--1581, 2007.

[36] T. Weis-Fogh, "Biology and Physics of Locust Flight. II. Flight Performance of the Desert Locust (Schistocerca gregaria)," *Philosophical Transactions of the Royal Society of London. Series B*, vol. 239, no. 667, pp. 459-510, 1956.

[37] M. May, "Aerial defense tactics of flying insects," *American scientist*, vol. 79, no. 4, pp. 316--328, 1991.

[38] R. Sahai, K. C. Galloway, M. Karpelson and R. J. Wood, "A flapping-wing micro air vehicle with interchangeable parts for system integration studies," *2012 IEEE/RSJ International Conference onIntelligent Robots and Systems (IROS)*, pp. 501--506, 2012.

[39] W. Bejgerowski, A. Ananthanarayanan, D. Mueller and S. K. Gupta, "Integrated Product and Process Design for a Flapping Wing Drive Mechanism," *Journal of Mechanical Design*, vol. 131, no. 6, 2009.

[40] J. A. Roll, B. Cheng and X. Deng, "Design, Fabrication, and Experiments of an Electromagnetic Actuator for Flapping Wing Micro Air Vehicles," in *IEEE International Conference on Robotics and Automation (ICRA)*, Karlsruhe, Germany, 2013.

[41] B. Cheng, J. A. Roll and X. Deng, "Modeling and Optimization of an Electromagnetic Actuator for Flapping Wing Micro Air Vehicle," in *IEEE International Conference on Robotics and Automation (ICRA)*, Karlsruhe, Germany, 2013.

[42] W. Shyy, Y. Lian, J. Tang, D. Vileru and H. Liu, Aerodynamics of Low Reynold Number Flyers, Cambridge: Cambridge University Press, 2008.

Gih-Keong Lau received his bachelor and master degrees in mechanical engineering from Nanyang Technological University, Singapore, in 1998 and 2001 respectively. He received his PhD degree of mechanical engineering in 2007 from the Delft University of Technology. Since 2008, he has been an assistant professor with the School of Mechanical and Aerospace Engineering, at Nanyang Technological University. His research interests are in the areas of micro-electro-mechanical actuators, electro-active polymers, compliant mechanisms, and bio-inspired micro-air vehicles.

Yao-Wei Chin received the B. Eng degree in aerospace engineering from the Nanyang Technological University (NTU), Singapore in 2010. He joined NTU as a Project Officer from 2010 to 2012. Since 2012, he is currently pursuing his Ph.D. research in the research group of Asst Prof. Lau Gih Keong. His research interests include bio-inspired flapping-wing flight, compliant mechanisms and fabrication of aerospace composites.

Joel Tian-Wei Goh received his bachelor degree in aerospace engineering from the Nanyang Technological University, Singapore in 2012. He assisted in the research and development of bio-inspired micro air vehicles prototypes as part of his final year project and subsequently as a temporary research assistant. Joel continues to be be interested in Aerospace/Aviation technologies. He is currently an executive in one of Singapore's major airlines.

Robert J. Wood received his master’s and Ph.D. degrees from the Department of Electrical Engineering and Computer Sciences at the University of California, Berkeley in 2001 and 2004 respectively. He is currently the Charles River Professor of Engineering and Applied Sciences in the School or Engineering and Applied Sciences and the Wyss Institute for Biologically Inspired Engineering at Harvard University. His research interests include microrobotics, bioinspired robots, and soft robots.